Comparison of Geometry-Based Transformer Iron-Core Models for Inrush-Current and Residual-Flux Calculations

R. Yonezawa, T. Noda

Abstract--**When a transformer is energized, a voltage drop is observed due to the inrush currents. An accurate transformer model that can reproduce the inrush currents is required for precisely assessing the voltage drop. Since the magnitude of the inrush current is affected by the iron-core magnetizing characteristics and iron-core geometry, the modeling of the iron-core magnetizing characteristics and the representation of the iron-core geometry are the two key factors in developing an accurate transformer model. In this paper, the inrush currents and residual flux are calculated using a newly proposed iron-core magnetizing model and a geometry representation, and the results are validated by comparison with laboratory test results.**

Keywords: **Transformers, Inrush currents, Residual flux, Magnetizing circuit, Iron-core geometry, and Electromagnetic transient (EMT) simulations.**

I. INTRODUCTION

When a transformer is energized, a voltage drop is observed due to the inrush currents [1]. From the viewpoint of power quality, an accurate transformer model that can reproduce the inrush currents is required for precisely assessing the voltage drop. Now then, residual flux is usually set 80 % of the rated flux for calculating the worst case in the analysis of the inrush currents [2]. However, if a transformer model is able to reproduce accurate residual flux, it becomes possible to set practical residual flux and to calculate appropriate inrush currents. Thus, a transformer model is required to reproduce not only inrush currents but also residual flux. Since the magnitude of the inrush current and residual flux are affected by the iron-core magnetizing characteristics and iron-core geometry, the modeling of the iron-core magnetizing characteristics and the representation of the iron-core geometry are the two key factors in developing an accurate transformer model.

An Iron-core magnetizing characteristic can be represented by the magnetizing circuit in Steinmetz's transformer equivalent circuit. Existing magnetizing circuit models can be divided into two classes: behavior-based models and physics-based models. The parameter determination process for behavior-based models is relatively simple, but these models

cannot accurately reproduce the residual flux, which may have a significant effect on the magnitude of the inrush current. The Chua model [3], which consists of a nonlinear resistance and a nonlinear inductance connected in parallel, is one of the most well-known behavior-based models. On the other hand, the physics-based models can reproduce residual flux after de-energization, but their parameter determination process is quite complicated [4]. The Jiles-Atherton model [5], [6] and Preisach model [7], [8] are examples of physics-based models. To overcome the limitations of two types of model, a behavior-based model that is capable of reproducing the residual flux has recently been proposed [9]. This model consists only of linear and nonlinear RLC elements, and their parameters can be determined in a simple way using information obtained from the nameplate, test report, and current-flux curve. It has been shown that the model precisely reproduces laboratory test results in terms of the inrush currents and residual flux [9].

The other key to developing an accurate transformer model is to represent of the iron-core geometry. Many power transformers have a three-legged iron core or five-legged iron core; these iron-core geometries are not three-phase symmetrical. To accurately reproduce the magnetic flux paths through the iron core, it is necessary to model the magnetic circuit representing the iron-core geometry. The following three approaches can be used to represent the magnetic circuit: 1) the traditional approach [10], 2) the duality-based approach [11], [12], and 3) the gyrator-capacitor-based approach [13]-[15]. Although the equations describing these three representations are identical, their implementation is different in general-purpose electromagnetic transient programs and their ease of understanding by engineers is different.

In this paper, we compare the above three approaches to representing the iron-core geometry and propose to the use of the gyrator-capacitor-based approach owing to its ease of implementation and understanding. In addition, the inrush currents and residual flux are calculated using the proposed iron-core magnetizing model and the gyrator-capacitor-based approach, and the results are validated by comparison with laboratory test results.

II. MAGNETIZING CIRCUIT MODEL

This section briefly describes the magnetizing circuit model proposed in Ref. [9].

Figure 1 shows the magnetizing circuit model, which is composed of a non-linear inductance L_{mag}, a non-linear

R. Yonezawa and T. Noda are with Electric Power Engineering Research Laboratory, CRIEPI (Central Research Institute of Electric Power Industry), 2-6-1, Nagasaka, Yokosuka, Kanagawa 240-0196, Japan (e-mail: {yonezawa, takunoda}@criepi.denken.or.jp).
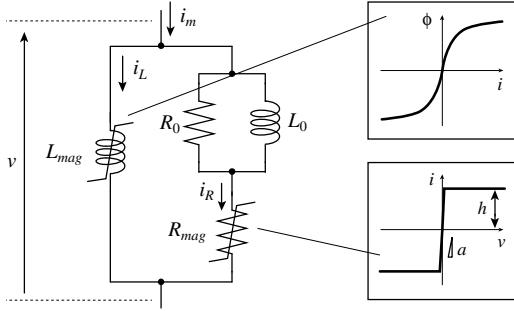
Fig. 1. The magnetizing circuit model has been proposed in Ref. [9].

resistance R_{mag}, a linear resistance R_0, and a linear inductance L_0. L_{mag} represents the magnetic saturation characteristic. R_{mag} represents the iron-core loss and is characterized by a low resistance (the slope of the voltage-current characteristic, a) when voltage across the model is small; otherwise it is characterized by the constant current h as shown in Fig. 1. R_0 and L_0 are elements that are included to perform smooth switching of the operation mode to be described later. R_0 is set to a value corresponding to the iron loss and L_0 is set to the time constant of L_0 and a is about 100 ms. The set value of h is obtained from the rated voltage V and R_0 using the following equation:

$$h = \frac{\sqrt{2}V}{R_0} \qquad (1)$$

The proposed model has four operating modes as shown in Fig. 2. C is the capacitance between the transformer winding and the ground.

A. Steady State

When the voltage across the model is sufficiently large, R_{mag} enters the constant-current ($= h$) mode. i_m is the sum of i_L and i_R (mode 1), where i_m is the magnetizing current, i_L is the current in L_{mag}, i_R is the current in R_{mag}. At this time, R_{mag} represents the iron loss because i_R flows through L_0 instead of R_0. When the voltage across the model is small, R_{mag} enters the low-resistance mode and i_R suddenly changes. At this time, i_R flows through R_0 because the impedance of L_0 is higher than that of R_0 (mode 2). R_0 represents the iron loss because R_{mag} is in the low-resistance mode. Therefore, the model repeatedly operates in mode 1 and mode 2 in the steady state, R_{mag} and R_0 represent the iron loss in modes 1 and 2, respectively.

B. After De-Energization

If a high voltage appears after de-energization, the impedance R_{mag} will be larger than the impedance C and L_{mag} since R_{mag} enters the constant-current mode. Thus, most of the current flowing through the circuit flow only L_{mag} and C, and a natural LC response appears (mode 3). After the ringdown transient has converged, R_{mag} enters the low-resistance mode. Since i_R changes slowly, i_R flows through L_0 instead of R_0. Consequently, the circulating current continues flowing between R_{mag} and L_{mag} for a long duration because R_{mag} is in the low-resistance mode (mode 4).

In fact, the residual flux is a static magnetic phenomenon in the iron core; this magnetizing circuit model represents it

using the continuous current. As noted above, owing to the two operation modes of R_{mag}, this model is capable of the representing two different conditions: the steady state and the condition after de-energization.

The parameters for the model are determined in a simple manner using information obtained from the nameplate, test report, and current-flux curve. The detailed parameters of transformers, such as the number of turns of the winding and iron-core size, are usually not available. But the information of name plate, test report and current-flux curve are available in many cases.

III. REPRESENTATION OF IRON-CORE GEOMETRY

In this section, the three approaches to modeling the magnetic circuit, the traditional approach, the duality-based approach, and the gyrator-capacitor-based approach, are compared.

A. The Traditional Approach

The traditional approach to representing a magnetic circuit is to use a reluctance-resistance analogy [10]. The magnetomotive force (MMF) $\mathscr{F}$ is regarded as being analogous to the voltage and the magnetic flux Φ as being analogous to the current. Figure 3 shows a single-phase two-winding transformer circuit representing the electrical circuit and the
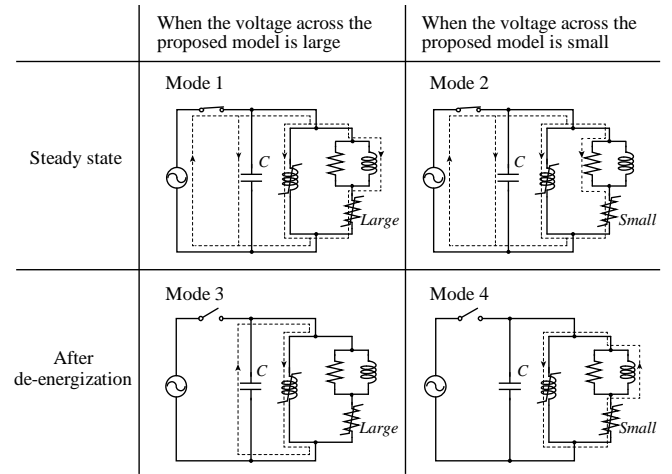
Fig. 2. The proposed magnetizing circuit model has four operating modes.
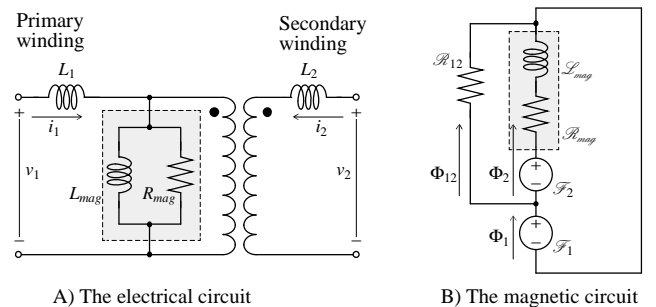
Fig. 3. A single-phase two-winding transformer circuit representing the electrical circuit and the magnetic circuit using the traditional approach.

magnetic circuit using the traditional approach assuming that it is not considered the winding resistance and the magnetizing circuit is represented by a linear resistance and a linear inductance. The parts indicated by the dotted line in Fig. 3 are the magnetizing circuit. The magnetic circuit can represent the leakage flux Φ_{12} as leakage magnetic paths, but an electric circuit cannot represent it directly. The leakage inductance is distributed to the primary side L_1 and secondary side L_2. The inductance L in the electric circuit is converted into reluctance $\mathscr{R}$ in the magnetic circuit, and the resistance R in the electric circuit is converted to the magnetic inductance $\mathscr{L}$ in the magnetic circuit. The value of each element is transformed using the following equations:

$$\mathscr{R} = \frac{N^2}{L}, \quad \mathscr{L} = \frac{N^2}{R} \tag{2}$$

where N is the number of turns of the winding. The connections in series in the electric circuit are converted into parallel in the magnetic circuit, and vice versa. An example of the magnetic circuit of a two-winding, three-phase, three-leg transformer is shown in Fig. 4 [12]. $\mathscr{R}_{\text{leg}}$ and $\mathscr{R}_{\text{yoke}}$ are the nonlinear reluctances of the transformer limb and yoke, respectively. $\mathscr{R}_{12}$ is the linear reluctance of the leakage paths between the primary and secondary windings, $\mathscr{R}_{2C}$ is the linear reluctance of the leakage paths between the secondary (inner) winding and the iron core, $\mathscr{R}_0$ is the linear reluctance of the zero-sequence leakage, and $\mathscr{F}_1$ and $\mathscr{F}_2$ are the MMF for induced by the primary and secondary windings, respectively. The magnetic circuit represented using the traditional approach is capable of preserving physical topologies, making it easy to intuitively understand. However, it should be noted that the losses are represented by inductors, unlike in an electric circuit. In the implementation of a magnetic circuit using the traditional approach in general-purpose electromagnetic transient programs, it is possible to represent the coupling between the electric circuit and the magnetic circuit using the following three components: 1) a current-controlled voltage source relating the MMF in the magnetic circuit and the winding current; 2) a differential circuit used to calculate the rate of change of the magnetic flux flowing in the magnetic circuit; 3) a voltage-controlled voltage source relating the winding voltage and the rate of change of the magnetic flux.
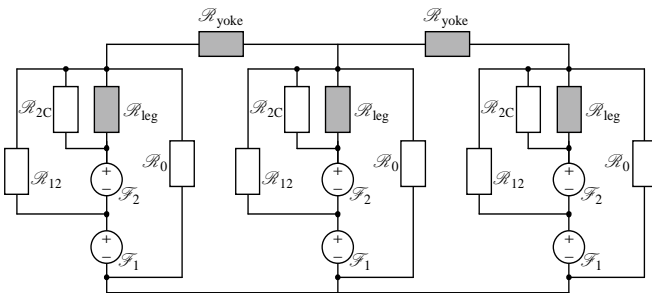
B. The Duality-Based Approach

The duality-based approach to representing the magnetic circuit is to use an electric circuit that has been converted from a magnetic circuit using duality theory [11], [12]. The equivalent electric circuit in Fig. 5 is obtained by the duality transformation of the magnetic circuit in Fig. 3. The value of each element is transformed using the following equations:

$$\mathsf{L} = \frac{N^2}{\mathscr{R}} = L, \quad \mathsf{R} = \frac{N^2}{\mathscr{L}} = R \tag{3}$$

This approach can be directly used for each element in the electrical circuit. The equivalent electric circuit in Fig. 6 is obtained by the duality transformation of the magnetic circuit in Fig. 4. Unlike the traditional approach, magnetic paths become nodes, and vice versa, since the physical topologies are not preserved. Therefore, some effort is required to transform the circuit and to the obtained result. In the implementation of the magnetic circuit using the duality-based approach in general-purpose electromagnetic transient programs, it is possible to represent the coupling between the electric circuit and the magnetic circuit using the following two components: 1) a current-controlled current source relating the current in the magnetic circuit and the winding current; 2) a voltage-controlled voltage source relating winding voltage and the voltage in the magnetic circuit. In practice, the pair of control sources is the same as that in an ideal transformer itself. Therefore, it can be implemented using ideal transformer components.

C. The Gyrator-Capacitor-Based Approach

The gyrator-capacitor-based approach to representing the magnetic circuit is to use a reluctance-capacitance analogy [13]-[15]. The MMF is regarded as being analogous to the voltage and the rate of change of the magnetic flux $\dot{\Phi}$ as being analogous to the current. The circuit representing the one of Fig. 3 in the gyrator-capacitor-based approach is shown in Fig. 7. R in the electric circuit is converted into conductance
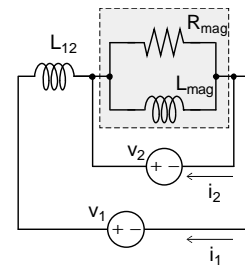
Fig. 5. The equivalent electric circuit obtained by the duality transformation of the magnetic circuit in Fig. 3.
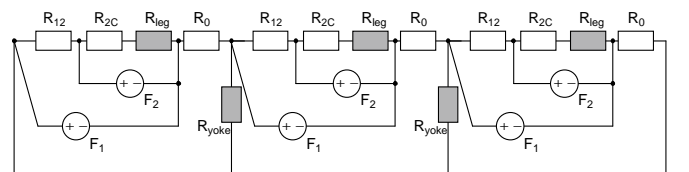
Fig. 6. The equivalent electric circuit obtained by the duality transformation of the magnetic circuit in Fig. 4.

Fig. 4. An example of the magnetic circuit of a two-winding, three-phase, three-leg transformer using the traditional approach.
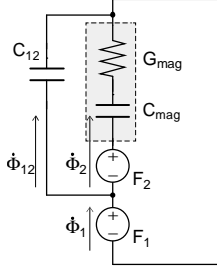
Fig. 7. The equivalent electric circuit obtained by the gyrator-capacitance-based approach of the electric circuit in Fig. 3.

G in the magnetic circuit, and L in the electric circuit is converted to the magnetic capacitance C in the magnetic circuit. The value of each element is transformed using the following equations:

$$\mathsf{C} = \frac{N^2}{L}, \quad \mathsf{G} = \frac{N^2}{R} \qquad (4)$$

In this approach, it is difficult to intuitively understand that the inductance is converted to the capacitance. However, the physical topologies are preserved, and the losses are represented as a resistance. Furthermore, the product of the across variable and the through variable is the power, consistent with the electric circuit. (The product of the across variable and the corresponding through variable is the energy in the traditional approach.) In the implementation of a magnetic circuit using the gyrator-capacitor-based approach in general-purpose electromagnetic transient programs, it is possible to represent the coupling between the electric circuit and the magnetic circuit using the following two components: 1) a current-controlled voltage source relating the winding current and the MMF in the magnetic circuit; 2) a current-controlled voltage source relating the rate of change of the magnetic flux flowing in the magnetic circuit and the winding voltage. The component with the pair of control sources that can invert the relationship between the voltage and current of the two circuits is called the gyrator. Thus, this approach is called, gyrator-capacitor-based approach.

A summary of the features of three methods of representing the magnetic circuit is given in Table I. Although the equations describing these three representations are identical because they only convert the variables, there are some differences as described above. We propose the use of the gyrator-capacitor-based model to represent the magnetic circuit because the physical topologies are preserved, the losses are represented as resistances, and differential circuits are not required.

IV. VERIFICATION

In this section, the inrush currents and residual flux are calculated using the proposed iron-core magnetizing model and the gyrator-capacitor-based approach, and the results are compared with those of laboratory tests for validation. The specifications of the test transformer used in the verification are shown in Table II. The experimental setup is shown in Fig. 8. The test transformer is a dry-type transformer, and the capacitance between the windings and the housing is smaller than that of typical oil-insulated power transformer. To simulate a typical power transformer, capacitances of 10,000 pF are connected between the primary winding terminal and the ground of each phase. The neutral point on the primary side is grounded using a 470 Ω resistor. Figure 9 shows the circuit of the test transformer using the gyrator-capacitor-based approach. The electric circuit is connected to the winding resistances R_{w1}, and R_{w2} of each winding. The magnetic circuit is connected the proposed magnetizing circuit, and C_{12} representing the leakage paths corresponding to each leakage inductance L_{12}. $\mathscr{R}_{2C}$ and $\mathscr{R}_0$ in Fig. 4 are assumed to be sufficiently larger than the magnetic reluctances of the iron core and are removed from the model in Fig. 9. Because the number of turns of the primary winding N_1 and the number of turns of the secondary winding N_2 are unknown, N_1 is assumed be $V_1/\sqrt{3}$ and N_2 is assumed V_2 because the ratio between the number of turns of the windings and the ratio between the voltages are subequal. The characteristics of C_{mag} and G_{mag} are shown in Fig. 10 and the value of G_0 is 4.57 [S], and C_0 is 61.4 [μH]. Owing to the effect of the yoke, the phase b corresponds to the center-leg winding and the other phases have different current-flux characteristics [16]. However, in this simulation, all three phases are applied to the $i - \Phi$ characteristic of the phase b winding. G_{mag} is approximated by

TABLE I
A SUMMARY OF THE FEATURES OF THREE METHODS OF REPRESENTING THE MAGNETIC CIRCUIT.

	Electrical domain	Magnetic domain		
		The traditional approach	The duality-based approach	The gyrator-capacitor-based approach
The across variable	Voltage [V]	MMF [A]	Voltage [V]	MMF [A]
The through variable	Current [A]	Magnetic flux [Wb]	Current [A]	Magnetic flux rate [Wb/s]
The product of the across variable and the through variable	Power [W]	Energy [J]	Power [W]	Power [W]
The element of representing the iron loss	Resistance	Inductance	Resistance	Resistance
The physical topologies	-	Preserve	Not preserve	Preserve
The coupling of the electric circuit and magnetic circuit	-	A differential circuit and two controlled soruces	An ideal transformer (two controlled sources)	A gyrator (two controlled sources)

		unit	Tr 1
Winding connection		–	Y–Δ
Rated power	S	VA	500
Rated voltage (HV)	V_1	V	200
Rated voltage (LV)	V_2	V	60
Frequency	f	Hz	50
No-load loss	W_o	W	13.7
Load loss	W_s	W	20.7
Impedance voltage	V_s	V	8.32
Leakage inductance	L_{12}	mH	1.04
Winding resistance (HV)	R_{w1}	Ω	1.80
Winding resistance (LV)	R_{w2}	Ω	0.434
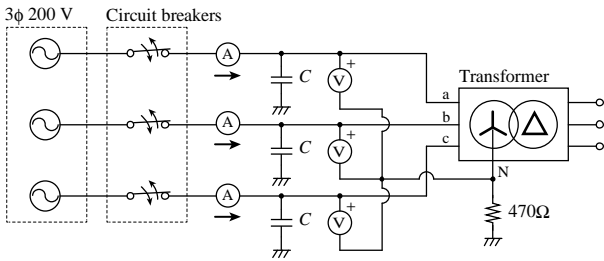
Fig. 8. The experimental setup.
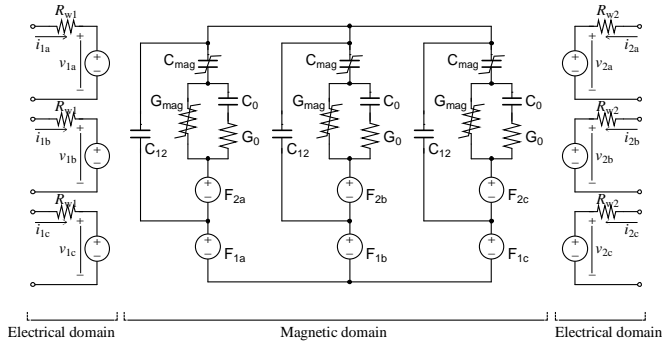
Fig. 9. The circuit of the test transformer using the gyrator-capacitor-based approach.
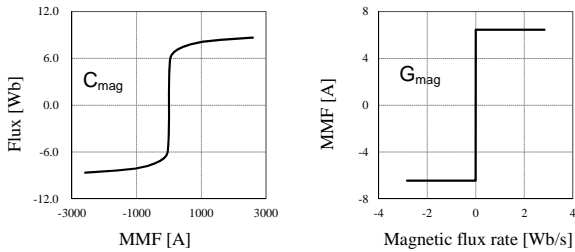
Fig. 10. The characteristics of C_{mag} and G_{mag}.

a nonlinear resistance, and a sufficiently large value compared with G_0 is set as the slope of the constant-current portion. The EMT analysis program XTAP (eXpandable Transient Analysis Program) [17] is used in these simulations.

A. Residual Flux

A typical circuit breaker can generally turn off when the current becomes zero. However, it might turn off at a nonzero current since the magnetizing current is quite small as the transformer is not subjected to a load. The voltage, current, and flux waveforms of the primary winding when the circuit breakers of each phase are simultaneously turned off from the steady state are shown in Fig. 11. The flux waveforms are calculated from the measured voltage waveforms by numerical integration. The phenomenon that the residual flux is retained after the circuit breakers are turned off is represented, and the values of residual flux of each phase have similar values to the measured values. Figure 12 shows an enlarged view of Fig. 12 around the region where the circuit breakers are turned off. Overvoltages appear after the circuit breakers are turned off because the breakers cut small currents. These phenomena are reproduced in the simulation results, but the magnitudes of the overvoltage are smaller than the measured values. This simulation takes into account the iron-core geometry but not the different of the $i - \Phi$ characteristics between the center leg and the other leg. This is considered to be one of the causes of the differences between the measured and calculated results.

In addition, the results when the circuit breakers of each phase are turned off at current zeros are shown in Fig. 13. The overvoltages do not appear in this condition, and the values of residual flux of each phase have similar values to the measured values.
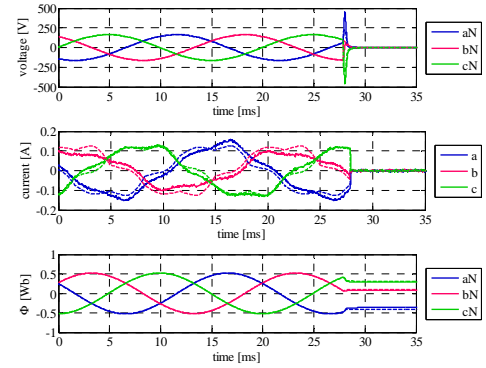
Fig. 11. The voltage, current, and flux waveforms of the primary winding when the circuit breakers of each phase are simultaneously turned off from the steady state (Solid line: measured, dashed line: calculated).
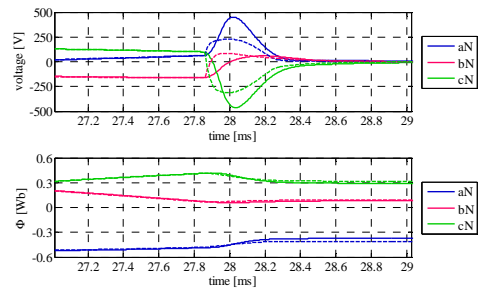
Fig. 12. An enlarged view of Fig. 12 around the region where the circuit breakers are turned off (Solid line: measured, dashed line: calculated).
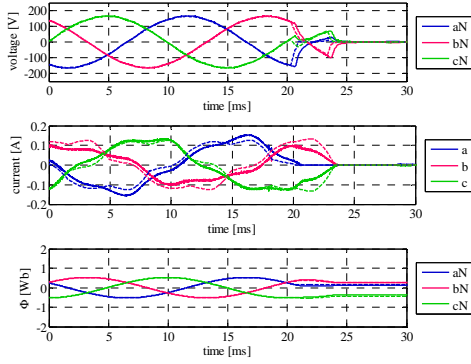
Fig. 13. The voltage, current, and flux waveforms of the primary winding when the circuit breakers of each phase are turned off at current zeros (Solid line: measured, dashed line: calculated).
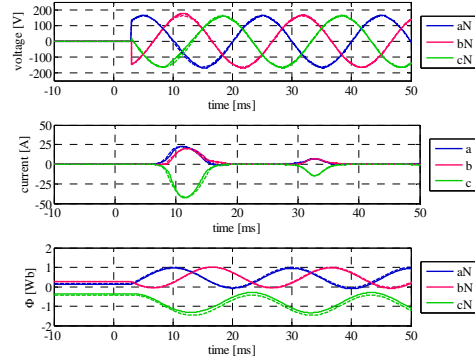
Fig. 14. The voltage, current, and flux waveforms when the energization occurs at 54° (Solid line: measured, dashed line: calculated).

B. Inrush Currents

The inrush currents are measured under the condition after the circuit breakers of each phase are turned off at current zeros. The timing of the energization is varied from 0 to 360° with increments of 18°. In simulations, the same simulation case in the previous section is used. The computation is proceeded for 20 ms from the de-energization timing, and the next timing that the voltage of phase a becomes 0° is regarded as 0° in this simulations. The residual flux of phase c (absolute value) is the largest among all phases in these experiments. In this case, it is expected that the inrush current will be largest when the voltage of phase c is energized at 180° (60° for phase a). Figure 14 shows the voltage, current, and flux waveforms when the energization occurs at 54°. The measurement results and calculated results are in good agreement. The peak values (absolute value) of the inrush current of each phase at each timing are shown in Fig. 15. As predicted above, the peak inrush current occurs when the energization occurs at approximately 60°, and it is possible to confirm the same tendency in the calculation.

V. Conclusions

In this paper, transformer models that take into account the iron-core geometry and can be used for inrush current and residual flux calculations are described. The three approaches to modeling the iron-core geometry are compared and the use of the gyrator-capacitor-based is proposed owing to its ease of implementation and understanding. It was shown that the proposed magnetizing model with the magnetic circuit model using the gyrator-capacitor-based approach precisely reproduces laboratory test results for the inrush currents and residual flux.

VI. Further Work

In this paper, we have only validated the proposed model using the small transformer not an actual transformer. Thus, we will carry out the proposed model validation using actual power transformers.
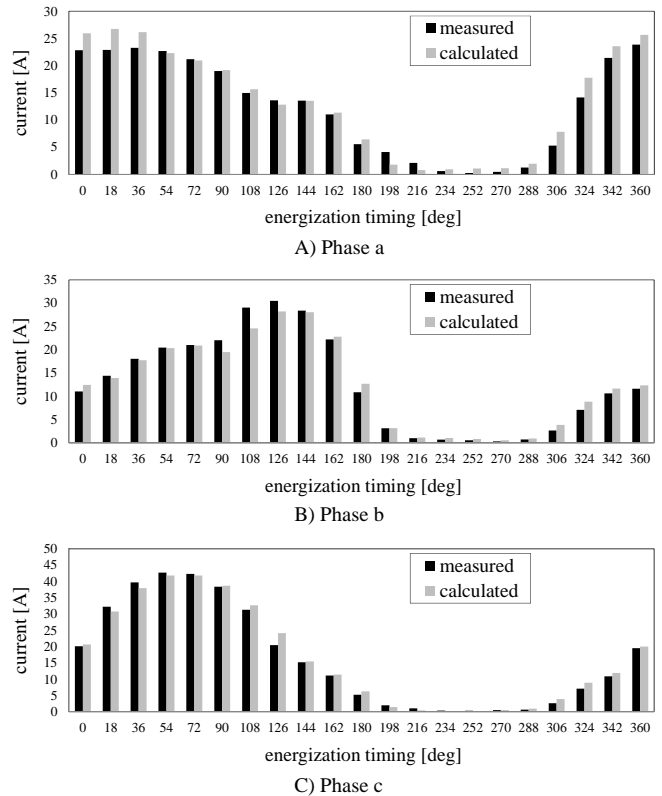
Fig. 15. The peak values (absolute value) of the inrush current of each phase at each timing.

VII. References

[1] L. F. Blume, G. Camilli, S. B. Farnham, and H. A. Peterson, "Transformer magnetizing inrush currents and influence in system operation," AIEE Trans., vol. 63, no. 6, pp. 366-375, 1944.
[2] CIGRE WG C4.307, "Transformer energization in power systems: a study guide," CIGRE Technical Brochure 568, Feb. 2014.
[3] L. O. Chua and K. A. Stromsmoe, "Lumped-circuit models for nonlinear inductors exhibiting hysteresis loops," IEEE Trans. on Circuit Theory, vol. CT-17, no. 4, pp. 564-574, Nov. 1970.

[4] N. Chiesa and H. K. Hoidalen, "Hysteretic iron-core inductor for transformer inrush current modeling in EMTP," 16th Power Systems Computation Conference (PSCC 2008), 2008.

[5] D. C. Jiles and D. L. Atherton, "Theory of ferromagnetic hysteresis (invited)", J. Appl. Phys., vol. 55(6), pp. 2115-2120, March 1984.

[6] D. C. Jiles, J. B. Thoelke, and M. K. Devine, "Numerical determination of hysteresis parameters for the modeling of magnetic properties using the theory of ferromagnetic hysteresis," IEEE Trans. Magnetics, Vol. 28, No. 1, pp. 27-35, Jan. 1992.

[7] F. Preisach, "Uber die magnetishe nachwrikung," Zeitschrift fur Physik, vol. B 94, pp. 277-302 1935.

[8] A. Rezaei-Zare, M. Sanaye-Pasand, H. Mohseni, S. Farhangi, and R. Iravani, "Analysis of ferroresonance modes in power transformers using preisach-type hysteretic magnetizing inductance", IEEE Trans. on Power Delivery, vol. 22, no. 2, pp. 919-929, April 2007.

[9] R. Yonezawa, T. Noda, N. Suzuki, H. Nagashima, F. Nomiyama, N. Yamaguchi, H. Honma, S. Kitamura, "Development of a Transformer Magnetizing Circuit Model for Inrush Current and Residual Flux Calculations," IEEJ Transactions on Power and Energy, vol. 134 no. 9, pp. 749-758, 2014.

[10] E. R. Laithwaite, "Magnetic equivalent circuits for electrical machines," PROC. IEE, vol. 114, no. 11, Nov. 1967.

[11] B. A. Mork, F. Gonzalez, D. Ishchenko, D. L. Stuehm, and J. Mitra, "Hybrid transformer model for transient simulation: Part I: Development and parameters," IEEE Trans. on Power Delivery., vol. 22, no. 1, pp. 248–255, Jan. 2007.

[12] N. Chiesa, B. A. Mork, H. K. Hoidalen, "Transformer model for inrush current calculations: simulations, measurements and sensitivity analysis", IEEE Trans. on Power Delivery, vol. 25, no. 4, Oct. 2010.

[13] D. C. Hamill, "Lumped equivalent circuits of magnetic components: the gyrator-capacitor approach", IEEE Trans. on Power Electronics, vol. 8, no. 2, April 1993.

[14] A. D. Brown, J. N. Ross, K. G. Nichols, "Time-domain simulation of mixed nonlinear magnetic and electronic systems", IEEE Trans. on Magnetics, vol. 37, no. 1, Jan. 2001.

[15] J. Allmeling, W. Hammer, J. Schonberger, "Transient simulation of magnetic circuits using the permeance-capacitance analogy", IEEE workshop on control and modeling for power electronics (COMPEL), PS-01-5, 2012.

[16] E. F. Fuchs, Y. You, "Measurement of λ-i characteristics of asymmetric three-phase transformers and their applications", IEEE Trans. on Power delivery, vol. 17, no. 4, Oct. 2002.

[17] T. Noda, K. Takenaka, and T. Inoue, "Numerical integration by the 2-stage diagonally implicit Runge-Kutta method for electromagnetic transient simulations," IEEE Trans. on Power Delivery, vol. 24, no. 1, pp. 390-399, Jan. 2009.